INTL JOURNAL OF ELECTRONICS AND TELECOMMUNICATIONS, 2019, VOL. 65, NO.2 , PP. 217-228
Manuscript received November 19, 2018; revised April, 2019. DOI: 10.24425/ijet.2019.126304

A Study of Types of Sensors Used in Remote Sensing

Shweta Vincent, Sharmila Anand John Francis, Kumudha Raimond, and Om Prakash Kumar

***Abstract*—Of late, the science of Remote Sensing has been gaining a lot of interest and attention due to its wide variety of applications. Remotely sensed data can be used in various fields such as medicine, agriculture, engineering, weather forecasting, military tactics, disaster management etc. only to name a few. This article presents a study of the two categories of sensors namely optical and microwave which are used for remotely sensing the occurrence of disasters such as earthquakes, floods, landslides, avalanches, tropical cyclones and suspicious movements. The remotely sensed data acquired either through satellites or through ground based- synthetic aperture radar systems could be used to avert or mitigate a disaster or to perform a post-disaster analysis.**

***Keywords*—Disaster Management; Microwave sensors; Optical sensors; Remote Sensing**

I. Introduction

REMOTE Sensing refers to the science and technology used to gather information about an event's occurrence or a phenomenon, without establishing direct contact with it. Remote Sensing forms one of the most important and widely used forms of science for us to learn about the environment we live in, and also to detect any kind of activity which could have an adverse effect or pose a threat to us.

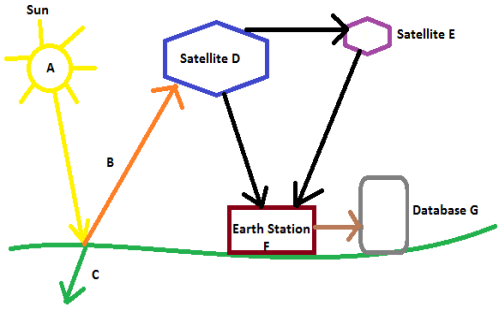

Fig. 1. Remote Sensing Architecture

Figure 1 illustrates a generic remote sensing system architecture. Component A in figure 1 is the sun considered as a source of illumination and energy. Components B and C illustrate the energy being reflected by the Earth's surface and also some being absorbed by the Earth. D and E are satellites used to receive and retransmit this reflected energy in order to detect features on the Earth's surface. F and G correspond to the usage of this data to generate understandable information such as Digital Elevation Models (DEM), raster and vector graphs etc.

A. Types of Remote Sensing based on source of energy used

Remote sensing can be divided into two categories based upon the source of energy used; active and passive. Active remote sensing is performed using a source that can emit energy, which when falls upon the object to be imaged/ detected, gets reflected back and leads to the detection of the object. On the other hand, in passive remote sensing, the source of energy used for detection of objects is the Sun. There is no other energy source that emits energy for object detection in the case of passive remote sensing.

B. Types of Remote Sensing based on the frequency used in the EM spectrum

There are several frequencies which constitute the electromagnetic (EM) spectrum. Each of these frequencies have their own characteristic wavelength and are used for a specific set of applications each. Figure 2 illustrates the EM spectrum.

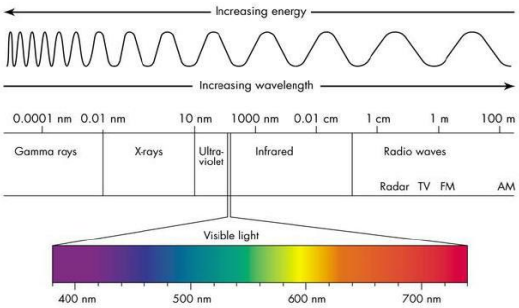

Fig. 2. The Electromagnetic (EM) Spectrum

In the case of remote sensing, the frequency bands in the EM spectrum can be divided into two broad domains; the optical domain and the microwave domain. The optical domain of frequencies consists of those present in the visible light spectrum i.e. waves with wavelengths between 400 nm and 700 nm. On the other hand, microwave frequencies range from 0.3 GHz to 40 GHz. Table I tabulates the various wavelength and frequency bands used in the optical and microwave remote sensing techniques.

The microwave domain is much preferred over the optical domain as it has a day-night visibility. Also, microwaves have the ability to penetrate through clouds and are thus very useful in detection of cyclones and hurricanes. Thus microwaves have an 'all-weather' capability.

Shweta Vincent is with Department of Mechatronics Engineering, Manipal Institute of Technology, Manipal Academy of Higher Education, Manipal and a PhD scholar at Karunya Institute of Technology and Sciences,Coimbatore

Sharmila Anand John Francis is with King Khalid University, Saudi Arabia

Kumudha Raimond is with Department of Computer Science and Engineering Karunya Institute of Technology and Sciences, Coimbatore

Om Prakash Kumar is with Department of Electronics and Communication Engineering, Manipal Institute of Technology, Manipal Academy of Higher Education, Manipal.

TABLE I
DETAILS OF THE OPTICAL AND MICROWAVE REGIONS OF THE EM SPECTRUM

Optical Infrared Region (OIR)		
Type	**Sub-type**	**Range**
Reflective	Visible	0.4 μm to 0.7 μm
	Near Infra-red	07 μm to 1.1 μm
	Shortwave Infra-red	1.1 μm to 3 μm
Thermal Infra-red		3 μm to 8 μm
Emissive	Long wave Infra-red	8 μm to 15 μm
	Far Infra-red	< 15 μm
Microwave Region (MR)		
Type		**Range**
P Band		0.3 GHz to 1 GHz
L Band		1 GHz to 2 GHz
S Band		2 GHz to 4 GHz
C Band		4 GHz to 8 GHz
X Band		8 GHz to 12.5 GHz
Ku Band		12.5 GHz to 18 GHz
K Band		18 GHz to 26.5 GHz
Ka Band		26.5 GHz to 40 GHz

C. Usage of remote sensing for detection of disasters

Remote sensing is the key technology used for the detection and early warning of several disasters such as earthquakes, floods, landslides, avalanches and cyclones. It can also be used for the detection of subtle forms of motion for life detection under a debris or could be used to thwart a terrorist attack by detecting concealed weapons. This article highlights a few of the various forms of disasters that can be mitigated and reported using various remote sensing techniques in the optical and microwave domain.

D. Structure of this article

Section 2 of this article throws some light on the research being carried out for remote sensing of earthquakes. Sections 3 and 4 describe the articles written for remote sensing of landslides and avalanches respectively. Section 5 gives details on remote sensing for detection of floods. Section 6 elaborates on the use of remote sensing data for early evacuation during tropical cyclones. Section 7 evaluates the various remote sensing articles written for detection of motion of humans and other objects. Finally, section 8 concludes the article.

II. REMOTE SENSING FOR EARTHQUAKE MONITORING

Sudden shaking of the ground due to movements in the Earth's crust is termed as an Earthquake. When tectonic plates of continents move due to some underlying activity in the mantle of the earth, then an earthquake occurs. This section of the article describes some of the many earthquake detection techniques which have been designed and implemented by researchers around the world.

A. Study of the impact of post-seismic activity on vegetation using MODIS

The Wenchuan earthquake which occurred in 2008 has been studied by Wentao *et. al*.[1] for measuring the change in the vegetation after the seismic activity of an earthquake. The authors of this article have collected data before and after the Wenchuan earthquake at a high spatial resolution level and on a high temporal basis. It has been found that post the earthquake, seismic activity has damaged the vegetation of the region due to induced landslides. In the due course of time it has been observed that the vegetation cover has increased and the post-seismic activity has died down. Wentao *et. al.* [1] have concluded that in the next two decades the post seismic activity in the region shall vanish completely. The MODIS satellite has been used to acquire the dataset for this study as it has a short revisit time of one or two days. Each image acquired by this satellite includes NDVI (Normalized Difference Vegetation Index) and a per pixel layer to show the validity of the NDVI data.

B. Damage mapping of the L'Aquilla earthquake of 2009 using QuickBird satellite

The L'Aquilla earthquake occurred in Italy in the year 2009. The QuickBird satellite images of VHR (Very High Resolution) have been used by Roberta *et. al*. [2] to assess the damage caused by this earthquake at the resolution of a single building. The authors have used the correlation techniques of Kullbach Leibler Distance and Mutual Information for analyzing the pre earthquake images and the post earthquake images. Their correlated data is compared with the *in situ* readings obtained from the QUEST (Quick Earthquake Survey Team). The Panchromatic and Multi spectral features of the VHR data have enabled the authors of this article to achieve a spectacular overall efficiency of 96.8%.

C. Validity of ALOS PALSAR (1 and 2) and Sentinel-1 data for deformation monitoring in Peru earthquake

Tazio *et. al.* [3] have presented a composite article by using several SAR satellite information for deformation monitoring in Peru. The data they have used has been gathered from ALOS (both 1 and 2),, PALSAR (both 1 and 2), ENVISAT ASAR and Sentinel-1 for mapping a total of 42 landslides that have occurred in the region. They have concluded that the ALOS PALSAR (1 and 2) and the Sentinel-1 sensors are capable of monitoring landslides caused by earthquakes at a rate of > 1 m/a which can't be detected by other sensors. This is due to the high revisit time of the aforementioned sensors and their sampling intervals as well as their wavelengths of operations.

D. Study of the Liquefaction hazards in Oklahoma using InSAR

William *et. al.* [4] have thoroughly studied the Pawning, Fairview and Cushing earthquakes which struck the USA in 2016. They have utilized the InSAR datasets to locate the epicenters of these earthquakes, determine the depth of the fault slips and determine the relationship of the fault slip with the location of the aftershocks. The dataset from the ESA's Sentinel-1a and 1b has been used which works in the C-band of microwave frequency range, due to the short revisit time and high spatial resolution. The InSAR observations are able to provide very precise assessment of the earthquakes and this has also been validated using *in situ* data.

E. CubeSat for damage assessment and recovery

Giancarlo *el. al.* [5] have explored the usage of constellations of satellites namely CubeSats for increasing the spatial resolution and the data accuracy for earthquake monitoring missions. Using an efficient method of architectural design can help nations to utilize the services provided by these satellites, though the resolution may not be suitable for precise monitoring. The authors of this paper have described the use of

CubeSats for covering a region in Brazil for disaster management post a natural calamity. They have tabulated the levels of spatial and temporal resolutions required for mitigation of various natural disasters. Giancarlo *et. al.* [5] have made use of satellites at two orbital planes inclined at an angle of 10 degrees at a height of 500 km to ensure the required revisit time. The communication systems of the CubeSat satellites operate using UHF receivers at a rate of 9600 bps. The authors have concluded by citing the pros of using CubeSat satellites as reduced cost of accessing the space for student activities and training.

F. Multi sensors to estimate Seismic vulnerability

Christian *et. al.* [6] have demonstrated the usage of multiple sensors to estimate the vulnerability of buildings using multiple sensor platforms namely; the RapidEye constellation, TandemX and Landsat. The data is acquired over the city of Istanbul in Turkey. The authors of this article have been able to establish a correlation between the predicted damage data and the *in situ* data with mean absolute errors of less than 11%. Christian *et. al.* [6] use multiple machine learning algorithms originating from Support Vector Machine (SVM) to come up with results.

G. Earthquake precursor detection through monitoring the Ionosphere

Kachikyan *et. al.* [7] have come up with a revolutionary article on detecting the precursors of earthquakes by monitoring the Ionosphere. They claim that earthquakes of magnitudes greater than 7 on the Richter scale can be detected well in advance by monitoring the ionospheric plasma in the region above the epicenter. They have concluded that by monitoring the F region of the Ionosphere continuously, the epicenters of strong earthquakes can be detected beforehand and early evacuation can be initiated. The authors have utilized the Interkosmos-19 satellite data from the ground ionosondes to form a mapping for the Irpinia earthquake that occurred in Italy in 1980.

H. Usage of Quickbird-2 satellite images for earthquake detection

Klonus *et. al.* [8] have utilized the Quickbird-2 images of Darfur in Sudan to devise an algorithm termed as Combined Edge Segment Texture (CEST) to automatically detect changes in a number of images obtained on a temporal basis to estimate the damage caused due to an earthquake that occurred in Darfur. An efficiency of 80% has been achieved using the CEST algorithm over other referenced algorithms in their article.

I. Usage of Ikonos and Spot 5 satellite imagery for earthquake detection

Andre *et. al.* [9] made use of the Ikonos images of the 2001 Gujarat earthquake to estimate the amount of damage caused. Their proposed algorithm is able to detect damages up to the level of individual buildings. They have also made use of images from Quickbird-2 and Spot 5 satellites.

Using the images of the Ikonos and Spot 5 satellites, Andre *et. al.* [9] have developed an algorithm with a false positive rate of 3.2% which was later on tweaked down to 1 %.

J. Using the Terra/ASTER and ALOS-PALSAR in ages for earthquake intensity estimation

Masafumi *et. al.* [10] have made use of the Terra-ASTER and ALOS-PALSAR images of the 2008 Siachuan earthquake of China to generate difference images of data acquired over a temporal basis. The algorithm works on finding the difference between two images captured one before the earthquake and one after it in order to estimate the amount of damage induced due to the earthquake.

K. 2.11 Use of Envisat-ASAR and TerraSAR-X for the study of the Tohoku - Oki earthquake

Salvatore [11] used both the Envisat-ASAR and TerraSAR-X to acquire data of the Tohoku – Oki earthquake which occurred on the 11th of March, 2011. Surface displacement was calculated at a RMS of 7.7 cms after some amount of calibration.

L. Use of Landsat-7 for Post-earthquake damage identification – Pakistan

S. J. H. Kazmi [12] has utilized the Landsat-7 images of Pakistan to create a damage estimate for an earthquake that rocked Pakistan in 2002. He concluded that, the Inverse Distance Weighted technique (IDW) can be used to develop a seismic risk map. Validation of his results with the Landsat-7 images was performed by field visits to Garhi Habibullah in Pakistan which was the base area for study in his article.

M. Quickbird-2 and Ikonos images for damage detection after an earthquake – Wenchuan earthquake

Tong *et. al.* [13] have used the Quickbird-2 and Ikonos images of shadows of buildings to estimate the extent of damage caused to the city of Dujiangyan during the 2008 Wenchuan earthquake. Using a generated 3 D model of the buildings in the area, the shadow regions of the image are calculated. Next the generated images is compared with the actual image of the region post-earthquake. A difference image generated from the previous two images estimates the amount of damage caused due to the earthquake. The efficiency of the proposed algorithm is 96.63%.

N. Usage of TerraSAR-X images for the detection of crustal movements – Tohuku earthquake

The Tohuku earthquake that occurred in 2011 in Japan has been analyzed by Wen Liu *et. al.* [4] using TerraSAR-X images. Shifting of buildings is calculated with pre and post earthquake images. Movements in the crust at a range of 0.32 meter to 0.12 meter were successfully detected in this article.

O. Usage of Ikonos images for assessing building damage in 3D

Xiaohua et. al. [15] have assessed the damage caused to buildings in 3 D using the Ikonos images. A Digital Elevation Model (DEM) is created using these images with an accuracy of 1.1 m in planimetry and 1.5 m in height. An overall accuracy of 90% for damage assessment during an earthquake is observed in this article.

Table II lists down the salient features of the satellites used for image acquisition and which have been used in the review articles described above.

TABLE II
A SUMMARY OF THE CHARACTERISTICS OF A FEW SENSORS

Name	Type of Orbit	Swath	Resolution	Type of Image	Special features
Quickbird – 2 [2] [8] [13]	Geosynchronous	15 km at 400 km altitude 34 km at 900 km altitude	0.61m panchromatic 0.4m multispectral	Panchromatic and Multispectral	Ball High Resolution Camera (BHRC 60) camera provides a Field of view of 2.12o.
Ikonos [9] [13] [15] [29]	Geosynchronous	11 km at nadir	0.82m panchromatic 3.2m multispectral	Panchromatic and Multispectral	First very high resolution (VHR) civilian sensor
TerraSAR-ASTER [10]	Sun synchronous	60 km	15 m to 90 m 14 multiple resolutions	Infrared	Enables creation of Digital Elevation models (DEMs) Consists of the following telescopes: Visible Near Infrared (VNIR) Short Wave Infrared (SWIR) Thermal Infrared (TIR)
ALOS–PALSAR [3] [10] [23]	Sun synchronous	55 km average	7 m to 44 m	Panchromatic and Multispectral	Three remote sensing equipment: Panchromatic Remote-sensing Instrument for Stereo Mapping (PRISM) Advanced Visible and Near Infrared Radiometer type 2 (AVNIR-2) Phased Array type L-band Synthetic Aperture Radar (PALSAR)
Spot – 5 [9] [18]	Sun synchronous	60 m x 80 m at nadir	5m panchromatic 10m multispectral	Green, Red and Infrared	Remote sensing equipment: HRG (High Resolution Geometric) and HRS (High Resolution Stereoscopic) DORIS Antenna TT&C Antenna Payload Telemetry Antenna
Landsat – 7 [12]	Sun synchronous	98 km	15 m to 90 m	7 bands of Thematic Mapper + 1 panchromatic band	'Zoom' lens for change detection and calibration
Sentinel 1 [13]	Sun synchronous	80 to 250 km Swath	5 m by 20 m	C Band SAR	An SDRAM-based Data Storage and Handling Assembly (DSHA)
RapidEye [6]	Sun Synchronous	77 km	6.5 m	RGB and NIR	Collection of 5 satellites
TandemX [6]	Sun Synchronous	350 km	1 m to 100 m	X band	Collection of 2 satellites

III. REMOTE SENSING FOR LANDSLIDE MONITORING

The slippage of one layer for earth over the other due to excessive rainfall or an earthquake is termed as a Landslide. The detection of landslides cannot be done using top view images of the earth as is the case with satellite or air-borne imagery. For successful detection of landslides, the image needs to be taken from a side view of the hill where a landslide is likely to occur. Thus the Ground Based Synthetic Aperture Radar (GB-SAR) system was devised. This consists of a radar with a transmitter and receiver placed opposite to a hill where the landslide is likely to occur and hence needs to be monitored. The review of the articles below describes a few of the GB-SAR systems in existence and draws a comparison between them.

A. Usage of InSAR for detection of ground inflation leading to landslides

T. Kobayashi *et. al.* [16] have presented an article to describe the phreatic eruption using the InSAR at the Hokano volcano in Japan. Phreatic eruptions are a result of pressurized geothermal fluids at shallow levels of the ground. Their results show that prior to a phreatic eruption, ground inflation occurred at a slow speed of almost 5mm per month. Their results were able to demonstrate that, data pertaining to high spatial resolution deformation can be extensively used for detecting subsurface pressure conditions with a very good accuracy using the ALOS-2 SAR.

B. Updating of Landslide activity maps using A-DInSAR data

B. Roberta *et. al.* [17] have developed a new methodology termed as LAMBDA (Landslide state of Activity Maps by combining multi temporal A-DInSAR data). The satellite data used in this relation was of the ERS- 1 and 2, RadarSat 1 and 2 and Cosmo-SkyMed over the Alps. With a stability threshold of +1 to -1, the multisensory data was able to update the state of activity of landslides from 2014 to 507 out of the earlier assigned 1657.

C. Monitoring slow moving landslides in Peru

N. Bontemps *et. al.* [18] have investigated the usage of the SPOT 1/5 Pleides archive for monitoring slow moving landslides in Peru. They have studied the archived data of 28 years to present the interaction of climatic change kinetics with earthquakes. Their investigations suggest that the Maca earthquake of 1991 has an effect on the landslides in the Peru region and is accelerated by the increased threshold of precipitation in the region.

D. Precursor detection for landslides using Sentinel-2 data

The Sentinel-2 satellite's data which has a 5 day revisit time has been utilized by P. Lacronix *et. al.* [19] to identify precursors for the detection of landslides in the French Alps. Their analysis suggests a low activity period of 7 months followed by an accelerated activity of landslides within 3 days. The authors

have used the Voight's law for creeping materials to simulate the sudden acceleration of landslides with almost a 100% accuracy.

E. Usage of GB-SAR for selecting coherent pixels in landslide monitoring

Z. Wang et. al. [20] have proposed a novel technique of selecting pixels which are coherent in interferograms of InSARs so that the temporal complexity of the images obtained, for landslides, by the GB-SAR can be minimized. To validate their results, they have used MetaSensing's FastGBSAR system's data set which operates in the Ku band with a full spatial resolution and acquisition time of 10 seconds. The first data set is considered for King Edward's bay. The second is of Queen Elizabeth's Metro bridge. Finally using least squares inversion, the datasets are validated.

F. Using GF-1 satellite data for detecting landslides in cloud covered images

X. Chen *et. al.* [21] have investigated the results of using the GF-1 satellite image data for detection of landslides in images covered by clouds. By introducing a Basic Belief Assignment (BBA), the authors of this article have been able to show that their process of detection of landslides in a cloud cover is superior to the conventional method of performing change detection on the image after cloud removal. They have considered the Ludian County of the Yunnan province in China as their area of investigation.

G. Airborne DInSAR for landslide detection

N. Cao *et. al.* [22] have utilized an airborne DInSAR images over the Slumgullion landslide in Colorado for investigation of the extent of the landslide. They have proposed the usage of the Backprojection algorithm on the DInSAR images for deformation detection. To verify the performance of their system, they have cross validated their results using the satellite data from the Global Navigation Satellite System (GNSS) and the COSMO-SkyMed (CSK). They have concluded that a low cost L-band DInSAR has the possibility of generating deformation maps at a centimeter level which is very accurate.

H. ALOS PALSAR for 3D mapping of landslides

The ALOS PALSAR has been investigated for 3D mapping of landslides by P. Razi *et. al.* [23]. They have considered the West Sumatra region in Indonesia as their dataset. P. Razi *et. al*. have considered the usage of persistent scattering interferometry (PSI) of the ALOS PALSAR for the deformation monitoring. They have proved the validity of their results using in situ data and have achieved deformation monitoring with a mean error of 0.3% which is considerably very low.

I. LISA for monitoring of the Tessina landslide

Tarchi *et.al.* [24] have devised the Linear Synthetic Aperture Radar (LISA) to monitor the Tessina landslide in Italy which occurred in 1960. It uses a frequency of 17 GHz for operation and generates a synthetic aperture of 2.8 meters. It consists of a mechanical rail of a length of 2.8 meters on which a microwave system consisting of one pyramidal horn antenna used as a transmitter and another pyramidal horn antenna used as a receiver is present. Data of the opposite hill is acquired by the LISA systems in every 14 minutes. 400 raw data sets are collected from the system and processed further to obtain a real-time image of the opposite hill. This is done on a temporal basis and any slight variation in the topography of the acquired image is treated as a warning sign before the occurrence of a landslide. Thus the LISA system provides continuous, all-weather monitoring of landslides.

J. IBIS-L System (Image by Interferometric System-Landslides)

The IBIS-L system is similar to the LISA system in the way that it uses a moving coherent radar along a 2 meter to 3 meter mechanical rail. This also uses two horn antennas, one for transmission and the other for reception working in the Ku-band. Michele *et. al.* [25] have presented an article on the imaging of structures for deformation monitoring using the IBIS-L. It can detect images with a pixel displacement of 0.1 mm.

K. In-GB-SAR (Interferometric GB-SAR)

An Interferometric Ground-Based Synthetic Aperture Radar (In-GB-SAR) system has been developed and tested by M. Sato *et. al*. [26]. Small changes in a target placed opposite to the system can be detected here using the concept of differential interferometry. A radar system working in a range of frequencies from 50 MHz to 20 GHz is used. Two pyramidal horn antennas are used; one for transmission of the waves and the other for the reflectionof the waves. The scanning aperture is 20 m in the horizontal direction and 1.5 m in the vertical direction. A woodent house with a few cracks in the outer wall was used for testing of this system. Using the In-GB-SAR, small displacements and cracks in the outer wall of the house were detected successfully.

L. MMW-GB-SAR (Millimeter wave Ground based SAR)

The MMW-GB-SAR is yet another GB-SAR system engineered to detect foreign object debris (FOD) from airport runways. This system has been developed by E. Yigit *et. al* [27]. Millimeter wave imaging is used in this article for the detection of objects. The experiments were carried out at the range of 32 GHz to 36 GHz and 90 GHz to 95 GHz. Using a matched filter algorithm for image reconstruction, FOD-like targets could be located successfully.

Table III illusrates the characteristics of the GB-SAR systems used for landslide monitoring and Table IV describes the other sensors used for landslide monitoring.

TABLE III
CHARACTERISTICS OF A FEW GB-SAR SYSTEMS

GB-SAR System	Axis Length (m)	Center Frequency (GHz)	Antenna Type	Number	Azimuth Resolution (m)	Range Resolution (m)	Distance (m)
LISA [9], [13]	5	5.83	Horn	2	6	2.5	1000-2900
IBIS-L [10]	2	17.2	Horn	2	4.4	0.75	4000
In-GB-SAR [11]	NA	2-8.4	Horn	1	3.5	5	5
MMW-GB-SAR [12]	1	32-36	Horn	2	3.75	3	3

TABLE IV
CHARACTERISTICS OF A FEW SPACE BORNE SENSORS USED IN LANDSLIDE MONITORING

Name	Type of Orbit	Swath	Resolution	Type of Image	Special features
ALOS-2 SAR [16]	Sun Synchronous	55 km to 70 km	3 m to 10 m	L band	Spotlight, Strip map and Scan mode
ERS 1 & 2 [17] [40]	Sun Synchronous	100 km	10 km to 50 km	L Band	Radar Altimeter, Along Track Scanning Radiometer, SAR, Wind Scatterometer, Microwave Radiometer
RADARSAT 1 & 2 [17] [32] [51]	Near circular Sun synchronous	45 km to 500 km depending on beam modes	8 m x 8 m in StripMap mode	X band	Uses a slotted waveguide SAR antenna of 15 m x 15 m dimensions
Cosmo-SkyMed [17] [22]	Sun synchronous	10 km to 200 km	1 m to 15 m	X band	Spotlight, Stripmap and ScanSAR modes
Sentinel-2 [19]	Sun Synchronous	290 km	10 m, 20 m and 60 m	13 spectral bands	Agriculture, Land use and land change mapping

IV. REMOTE SENISNG FOR FLOOD MONITORING

Submergence of dry land caused due to excessive rainfall or an overflow of water in a river is termed as a Flood. The flooding of China in the year 1931 resulted in 4 lakh casualties. Setting up of early warning systems for evacuation of people from their homes before the disaster of a flood strikes is a very crucial task to reduce the impact of the damage caused. False interpretation of data related to a flood could be extremely disastrous. This section of the article highlights two techniques used for monitoring the extent of flooding using satellite images.

A. Flood mapping in the Bolivian Amazon wetlands

Flood mapping in the Bolivian Amazon wetlands using multi sensors has been explored by A. Ovando *et. al.* [28]. They have used data from the MODIS, ENVISAT- 2, and SARAL AltiKa Meters. By using these sensors, the authors of this article have been able to throw light on the frequency of occurrence of these floods and their character whether they are caused by exogenous reasons or endogenous reasons. The results of their study have enabled other researchers to arrive at conclusions related to the general ecosystem imbalances in the wetlands and look for methods to preserve them.

B. 3D Mapping of cities for flood mapping

The city of Dresden in Germany has been used as a dataset of investigation and 3D mapping for flood detection by K. Schroter *et. al.* [29]. The authors of this paper have performed predictions using the Random Forest algorithm. The results have been validated by considering *in situ* data obtained from the region. The IKONOS Geo Ortho Kit satellite images have been used as the base data set for their project after initial rounds of image correction and processing.

C. Reduction of flood risk using a global network

L. Alfieri *et. al.* [30] have proposed the usage of a global network of data centers for reduction of flood risk across the globe. They have described the benefits of having a Global Flood Partnership (GFP) of scientists and researchers across the globe to mitigate the risks of flooding. They have proposed the utilization of the data sets pertaining to flood produced by the Dartmouth Flood Observatory (DFO) using the TRMM Multi satellite Precipitation Analysis (TMPA) maps. The River Watch version 3.4 also uses the TRMM, AMSR-E and 2 and GPM data for flood monitoring and post disaster analysis. The authors of this article have considered several case studies to prove the usefulness and success of such a global flood monitoring system.

D. Flood risk management in Leh, Ladakh

A. B. Hart *et. al.* [31] have performed a study of publicly available satellite imagery for flood mapping and watersheds monitoring in the remote region of Leh in Ladakh. Leh has an extreme topography and is prone to different forms of geohazards. The data from ASTER, GDEM and SRTM for Leh have been used by the auhors for creating DEMs of watersheds in the region and assessing debris flow. They have also been able to map sources of rock fall areas through ground trothing which was not available through the satellite data.

E. Usage of SAR images for river level extraction

M. O. Sghaier *et. al.* [32] have presented an article on the usage of SAR imagery for the determination of river levels. This can serve as a precursor for early detection of floods in certain regions. They have made use of the RADARSAT-2 data over regions in Canada as their base data set. After applying an algorithm based on local texture estimation and global knowledge associated with the region in consideration, the authors of this article have been able to achieve an accuracy of around 98% with a precision of around 88% in three sites of the region.

F. Usage of Near real time images for monitoring floods in South China

G. Tang *et. al.* [33] have performed a comprehensive study of the floods which hit South China in 2016. They have proposed the usage of Near Real Time (NRT) images obtained using the NRT satellite products for precipitation measurement. The data is considered for 13 provinces of the region on an hourly and daily basis and a comparison of the NRT satellite products based on Mean Square Error (MSE) and Coefficient of Correlation (CC) has been considered. It has been observed that the GSMaP NRT and IMERG Late correlate best with the ground truth data of the region.

G. Flash flood prevention using TV-Sats

F. Mercier *et. al.* [34] have introduced a novel method to prevent flash floods using TV satellite signals. This attributes to the attenuation of TV signals which gets caused by rain drops in the air. These signals are usually in the Ku band of the Microwave spectrum of energy. The authors have been able to rebuild high resolution rainfall maps using this technique. The region of

consideration is over Paris. The RMSE of this configuration is within a range of 0.3 to 0.8 for different sites in Paris and different configurations such as the entire map, rainy areas map and dry areas map.

H. ConvNet for flood identification

K. Nogueira *et. al.* [35] have investigated the use of ConvNet (Convolutional Neural Networks) for flood identification in eight different regions spanning from June 2016 to May 2017. The imagery is chosen from satellite images of 320 x 320 pixels resolution. A base set of 462 images is used to train the network and finally the accuracy of the test obtained is an average Jaccard index of 80%.

I. TerraSAR-X images for real-time flood detection- Tewkesbury, Italy

A real-time flood detection mechanism has been put in place by Mason *et. al.* [36] which analyzes the 2012 flood of Severn/Avon in the town of Tewkesbury, Italy. The usage of TerraSAR-X images for this purpose is inevitable due to the day-night operational capability of it and also its capability to penetrate through clouds which are present over the area of interest during a flood. With some preprocessing to better the resolution of the images and speckle filtering, the mean SAR backscatter threshold is calculated. 75 % of all the images are correctly interpreted. There is a false negative percentage of 25% using this algorithm. The data processing time is recorded as 19.1 minutes.

J. Envisat-ASAR images for the creation of Grid technology in real-time flood detection

R. Cossou *et. al.* [37] have made use of the all-weather capability Envisat-ASAR images to develop the Fast Access to Imagery for Rapid Exploitation (FAIRE) grid. FAIRE provides fast access to highly distributed data at a single point which helps users to reduce their time in accessing images for damage estimation caused during any flood. Experimentation was done, using FAIRE for the flood that hit North East India on the 6th of August, 2007. The result came up to half a pixel residual mis-registration and 75 meters of geolocation error.

V. REMOTE SENSING OF TROPICAL CYCLONES

Cyclones are a common phenomenon over large bodies of water which are warm in temperature. The warm water of the oceans has a tendency to evaporate and when it reaches a certain height in the atmosphere, it cools down and condenses to form rain clouds and water drops. Cyclones also have to be monitored cautiously to prevent damage to life and property. This section reviews a few articles written on monitoring of tropical cyclones using satellite imagery.

A. Geospatial techniques for Cyclone assessment

M. A. Hoque *et. al.* [38] have performed a detailed assessment of the risks pertaining to cyclones hitting the Sarankhola Upazila region on the coast of Bangladesh. Three criteria namely, vulnerability, hazard and mitigation capacity have been considered for mapping according to their algorithm. They conclude by stating that the eastern, southern and the south western regions of the region under study have a higher volume of cyclone surges as compared to the other areas due to heavier rainfall and strong winds. The authors have used the Landsat 8 satellite for their study of this region.

B. Study of storm surges in China

X. Feng *et. al.* [39] have investigated the Zhejiang, Fujian and Guangdong provinces for the study of storm surges in China. They have created a grid model for these provinces using a coupled grid. They have used a dataset provided by the Center for Topographic studies of Ocean and Hydrosphere (CTOH) in France from 1997 to 2016. The authors conclude by stating that the maximum surge can reach up to 0.6 meters in a year with a confidence for 90%.

C. Eddy current detection using Deep Learning and Remote Sensing

Y. Du *et. al.* [40] have presented an article for automatic ocean eddy current detection. They have explored and presented the use of Deep Learning for the mapping of multiple features of eddies in order to detect and analyze them better. The authors have named their system as DeepEddy and have tested their system on 20,000 SAR images. For all the images, they have been able to attain an accuracy of detection for almost 97.8%. Images of ENVISAT and ERS-2 satellites have been used for their investigations.

D. Effects of cyclones on hydro-meteorological factors and agriculture

The Supercyclone of 1999 and Phalin of of 2013 caused large scale devastation on the east coast of India. B. R. Parida *et. al.* [41] have explored the effect of these cyclones on the hydro-meteorological factors and agriculture of the region. They have used the data from TMPA-3B42 satellite and daily data from the Indian Meteorological Department (IMD). Their study suggests that rainfall accompanied by peak discharge from the rivers in the adjacent areas were the major cause of flooding in the region which led to loss of life and property. This also affected the Kharif agricultural crop and reduced its production by a rate of 57%. The final conclusion of the article was that precipitation data acquired from satellites could be very beneficial in studying the effects of cyclones on hydro-meteorological factors and the agriculture of the region. The satellite data sets for this investigation were obtained from TRMM Multi Satellite Precipitation Analysis (TMPA).

E. Remotely sensing convective clouds

A. K. Mishra [42] is the sole author of an article related to the study of convective clouds which are the reason for causing heavy rainfall and triggering disasters. Current research focuses on the study of convective cloud behavior in the Near Infrared range using the MeteoSat First Generation (MFG). The author of this article has used the TRMM data of 19 years to validate his results and mapping. He obtained a coefficient of correlation of 0.73 and a standard error estimate of 2.96%. His study yields the statistical results that an increase of 41.56% increase in convective clouds is caused by every degree increase in the temperature over the Indian subcontinent.

F. Detection of a cyclone in a partially covered SAR image

S. Jin *et. al.* [43] have presented an article related to the detection of a cyclone in a partially covered SAR image through an algorithm based on matching. The eye of a cyclone can be easily detected in an image which is a clear SAR image.

However, in some cases, only a part of the cyclone gets covered without the eye being identified in the SAR image. In such a case, the authors of this article propose the usage of a matching algorithm to detect the eye of the cyclone. They have validated their results with NOAA National Hurricane Center's data. They have utilized the data acquired from RADARSAT-1 which provides images in the C-band. On comparing their predicted cyclone eye's with the results obtained by using Genetic algorithm and in situ data validation, the authors claim that the eye of the cyclone can be detected precisely.

G. Usage of small satellites for weather monitoring

Y. Ma *et. al.* [44] have proposed the use of 14 small satellites carrying microwave sensors to cover the entire Earth for providing data. Their proposed constellation is more cost effective in comparison to the existing satellite constellations in place to monitor the Earth. The authors have shown through simulations that by using their constellations, middle-altitude cyclones can be mapped very well.

H. Monitoring of the center of a typhoon [45]

T. Hu *et. al.* [45] have used the Feng Yun-2 (FY-2) satellite and microwave scatterometer Hai Yang-2 (HY-2) to detect the center of a typhoon successfully. The northwest region of the Pacific Ocean is chosen for study in this article due to a high rate of cyclones and typhoons hitting the region every year. The authors claim that both the FY-2 and HY-2 sensors are capable of detecting the centers of 9 such typhoons accurately.

I. Usage of TRMM for generating a relation between cyclone intensity and SST.

Akiyoshi *et. al.* [46] have used the Tropical Rainfall Measuring Mission (TRMM) satellite data to present an algorithm to find a relationship between a cyclone's intensity and sea surface temperature (SST). The data for experimentation has been collected from over the Pacific Ocean. It has been concluded in this article that tropical cyclones in the Pacific Ocean towards the west are 38.2% larger in intensity than in the east of the Pacific Ocean.

J. Cloud detection using the MODIS satellite

Brian *et. al.* [47] have presented an algorithm for the detection of clouds using the MODIS images over the Gulf of Mexico. The main motivation behind their work in this article is to clearly classify clouds correctly and not to misclassify pixels of sea glint as clouds. Therefore using their algorithm they have been able to detect clouds and mask them efficiently in order to finally provide a high SST coverage data. This system also has an all-weather capability.

K. NSS-6 satellite usage for prediction of rate of rain

Das *et. al.* [48] have utilized the NSS-6 images to predict the rate of rain in a tropical location based in a Gaussian distribution model for the conditional occurrence of rain. The mean error of the system designed by them is around 20%. There are a number of comparisons drawn with other rain predictors in this article.

L. Usage of TMMI instrument to generate a relation between SST and cyclone intensity

Similar to Akiyoshi *et. al.*[46], M. M. Ali *et. al*. [49] have used the data of the TMMI (Tropical Rainfall Measuring Mission Imager) to draw a relation between sea surface temperature (SST) and cyclone intensity over the Indian Ocean. They have carried out a study on 75 cyclones during the period of 1998 to 2011 and have concluded that in the Indian Ocean almost 50 % of cyclones have no relation with SST. Therefore they have stated the SST is not a justifiable parameter to monitor cyclones in the Indian Ocean.

TABLE V
A SUMMARY OF THE CHARACTERISTICS OF A FEW MICROWAVE SENSORS

Name	Resolution	Type of Image	Special features
Envisat ASAR [11] [37] [40]	Radiometric resolution of 1.5 dB to 3.5 dB	C band microwave	5 Polarizations VV, HH, VV/HH, HV/HH, VH/VV
TerraSAR-X [11] [14] [36]	Staring Spotlight – 25 cm High Resolution Spotlight – 1 m Strip Map – 3m ScanSAR – 18.5 m	X band microwave	2 D SAR images. Staring Spotlight sensor provides the highest resolution by any other instrument Uses a 4.78 m x 0.7 m active phased antenna
TRMM [30] [41] [42] [46] [49]	VIRS – 2.4 km TMI – 5.1 km PR – 5.0 km	S band microwave	Various radars available: Visible/ Infrared Scanner (VIRS) Lightening Imaging Sensor (LIS) Clouds and the Earth's Radiant Energy System (CERES)
MODIS [1] [28] [47]	250 m to 1000 m depending on respective spectral bands	36 microwave bands	Bands from 0.4 μm to 14.4 μm
NSS-6 [48]	RCS of 19.9526 sq.m.	Ku and Ka microwave bands	50 Ku and 12 Ka bands to span over Asia, Australia, Africa and the Middle East
Kalpana [50]	2 km x 2 km to 8 km x 8 km	C band Microwave	Planar VHRR antenna Three bands of imaging: Visible (VIS) Total Infrared (TIR) Water vapour (MWIR)
FY-2 [45]	1.25 km x 1.25 km to 5 km x 5 km	S band	Three bands of imaging: Visible (VIS) Total Infrared (TIR) Water vapour (MWIR)
HY -2 [45]	18 km to 100 km	S and X bands	Wind Speed, SST, Ice monitoring and Water vapour monitoring

M. Kalpana satellite for the detection of center of a cyclone

Neeru *et. al.* [50] have experimented on the images of a couple of cyclones that hit India namely the Phyan, Ward, Laila and Phet. Their algorithm is used to determine the center of the cyclone from the images of these cyclones sensed by the Kalpana satellite. The algorithm determines the point of convergence of the gradient vectors of the brightness temperatures around a point. The algorithm has been proven to detect the centers of these cyclones successfully with a mean error between 42 km to 82 km.

N. Usage of RADARSAT-1 for rectifying azimuth scalloping

Roland *et.al.* [51] have utilized the RADARSAT-1 imagery to overcome the problem of azimuth scalloping. They have devised a descalloping technique to be used on a processor for the RADARSAT-1 acquired images.

It is clear from the summary of the articles stated above, that for monitoring of cyclones, microwave sensors are preferred over optical sensors due to their all-weather capability and ability to penetrate through clouds. This key feature of microwave sensors makes them more useful to monitor climate change and perform weather forecasting. Table V lists down a few of the microwave sensors used for monitoring of cyclones and floods.

VI. REMOTE SENSING FOR MOTION DETECION

The detection of movement of a living or non-living being is important to decide upon its behavior. In the area of defense and life detection under the debris of a man-made structure detection of movement becomes very critical. This section of the article highlights some of the research articles written on the lines of motion detection.

A. Low complexity Doppler radar for motion detection

C. Gu *et. al.* [52] have proposed the Digital Post Distortion Technique (DPoD) for compensation of signal distortions in Doppler radar signals of the digital baseband domain which can be used to detect slow motions such as that of a heartbeat. Their results show that the proposed technique along with the Doppler radar can be used for precise detection of slow Doppler motions.

B. Doppler radar for respiration rate measurement

J. Tu *et. al.* [53] have investigated the usage of Doppler radar even while the subject to be monitored is in motion. In such cases, it becomes difficult to detect any slow Doppler motion such as for evacuation or lifesaving operations. The authors of this article have tapped the frequency spectrum of the body under motion and the direction of motion along with the breathing peaks can be calculated. They have used a 5.8 GHz non-contact continuous wave Doppler radar system on a slow moving body and have been able to detect it with an error of barely 7.15%.

C. Object positioning using FMCW radar

Y. Wang et. al. [54] have proposed the construction of a CMOS transceiver chip with a 2 GHz bandwidth with a center frequency at 15 GHz which can be used to sense objects and motions of human limbs. They claim that the chip draws a power of only 210 mW for its operation. It uses an FMCW (Frequency Modulated Continuous Wave) radar principle for transmission and reception. This technique has enabled the authors of this article to reduce the power consumption and increase the bandwidth of operation of their proposed chip in comparison to existing chips of different technological makes.

D. UWB radar for human motion detection

C. Ding *et. al.* [55] have presented an article citing the usage of an Ultra Wide Band radar (UWB radar) for the detection of human motion using machine learning algorithms of SVM (Support Vector Machine), Decision Trees and KNN (K-Nearest Neighbour algorithm). They have been able to achieve a detection classification efficiency of around 94% using the Subspace KNN algorithm for *in situ* movements and around 95% using the Principle Component Analysis (PCA) algorithm for Bagged Trees in the case of *non-in situ* movements.

E. Motion compensation in Doppler radar for a life sensor

R. H. Nakata *et. al.* [56] have proposed the usage of a motion compensation algorithm for a Doppler radar which is used on UAVs (Unmanned Aerial Vehicles) for life detection after a disaster. The movement of the Doppler radar causes the weak life signal to get corrupted due to the motion of the aerial platform which the radar is mounted. To overcome that, the authors of this article have made measurements using a stationary radar which is used to subtract the phase difference caused due to the motion of the radar of the aerial vehicle. The difference signal is able to life signs between 15 dB to 41 dB on the test bed and for 25dB on the aerial platform.

F. TerraSAR-X for Polarimetric analysis of land use detection

With the increasing demand of land for different purposes such as agriculture, building colonies, mining etc. the science of land use detection and utilization is gaining momentum. Armando *et. al.* [57] use analysis in the polarimetric domain to detect changes in the usage of land and its resources. Due to the all-weather capability of TerraSAR-X, they have used the images of this satellite for their analysis and design of datasets. Validation of results is done by comparing the results of their algorithm with ground data and they conform to the ground survey data.

G. Detection of pedestrians using Millimeter waves

Waves that occupy the microwave spectrum of 30 GHz to 300 GHz are termed as Millimeter waves. Mehrnoosh *et. al.* [58] have used these millimeter waves to build a system to detect pedestrians and hidden objects with people such as knives or guns. This can be done by studying the backscatter of the millimeter waves when they bounce back from the person. For objects which have sharp edges, the radar backscatter is different in comparison to the backscatter from smooth objects. Based on this the radar polarimetry algorithm is devised to detect objects which have a higher cross-polarized backscatter and are therefore classified as sharp concealed objects.

H. Usage of Noise radar for through the wall imaging system

Pinheng *et. al.* [59] have utilized the technology of a noise radar to carry out imaging of activity or objects across a wall or through the wall. A noise radar uses a noise signal for transmission. Optical reception is made use of to detect the echo signal of the noise radar transmitted waveform. In their article, Pinheng *et. al.* have been able perform imaging and ranging operations of even humans across walls up to a distance of

around 9 meters. A-priori data of a room's image across the wall without any human activity is taken as the reference image for subtraction.

I. Netted radar for target localization

The multistatic radar system or netted radar system is proposed by Sammartino *et. al.* [60] for localization of targets. In a multistatic radar system, a number of radars which could either be monostatic or bistatic are used in conjunction to each other to detect a common target. This requires a lot of data fusion to occur for all the data to converge. The authors in their article performed an analysis of centralized and decentralized localization schemes for target detection. A comparative analysis of all the schemes generates the inference that the numerical approach is much more robust than the centralized MIMO approach for target localization.

J. Slotted waveguide antenna for the design of CARMSAR

Yue Liu *et. al*. [61] have researched upon the usage of a slotted waveguide antenna to design and construct a radar termed as CARMSAR (Compact and Reconfigurable Miniature SAR). CARMSAR is a FMCW radar used for imaging. It has the dimensions of 30 cm x 15 cm x 3cm. with an azimuth and range resolution of about 0.15 m. The swath width and the slant range are equal to a value between 1 to 3 kms. The Range Doppler Algorithm (RDA) is used for imaging in the CARMSAR. Using a frequency of 9.6 GHz, this system was tested and yielded the result that it was able to image objects when mounted on a flight 20 meters above the ground moving at a velocity of 10 mps.

K. Detection of life using UWB radar

An UWB radar transmits signals in a wide frequency spectrum of the microwave domain. Yanyun *et. al.* [62] have proposed and approach in which the metric of a Constant False Alarm Ratio (CFAR) is calculated using the raw echo of the waveform sent for detection of life. After the operation of frequency averaging, a threshold is arrived at to find the value of the CFAR. Tests are now made to compare other received echos with this threshold value. Values above the threshold are considered as the detection of life and any other echos below the threshold are considered as a no life signal. Their algorithm has been able to detect life signs within signal with a signal to noise ratio (SNR) between 12 dB to 6 dB.

From the above section it is clear that there are a number of ways in which the detection of motion can be performed based upon the requirement. This section aimed at presenting a few forms of systems used for detection of any kind of movement. Table VI attempts at listing out the key characteristics of the radar described in the section above.

TABLE VI
A SUMMARY OF THE CHARACTERISTICS OF A RADARS USED FOR DETECTION OF MOTION

Name	Frequency of operation	Key characteristics of sensor used
Doppler Radar	Variable	Based on the Doppler effect
TerraSAR-X satellite [57]	X band	2 D SAR images. Staring Spotlight – 25 cm High Resolution Spotlight – 1 m Strip Map – 3m ScanSAR – 18.5 m
Millimeter waves radar [58]	30 GHz to 300 GHz	Transmit a large amount of data. Line of sight needed for transmission. Maximum distance that can be covered is 1 km.
Noise radar [59]	1030 MHz to 1060 MHz	Uses a Log Periodic Dipole Antenna (LPDA) for transmission
Netted radar [60]	2.4 GHz	Uses both monostatic and bistatic radars. High coverage area. High spatial resolution due to spatial diversity. Requires more processing
FMCW [54] [61]	9.6 GHz	Uses a FMCW radar with a slotted waveguide of 30 cm x 15 cm x 3 cm dimensions Linear polarization. Low cross polarization.
Ultra wide band radar [55] [62]	Bandwidth of 2 GHz	Wide frequency range. Transmitted pulses need to be of a very short duration.

VII. CONCLUSION

This study article presented a few of the various sensors used for remotely sensing disasters. Their frequency of operation as well as some of their special features highlighted. The aim of the study was to emphasize on the various types of microwave and optical domain sensors used for data acquisition during disasters. Though no study as such can encompass the entire realm of disaster management using remote sensing, a humble attempt was made in this article to uncover some of the critical characteristics of optical and microwave sensors used during disaster management.

REFERENCES

[1] Y. Wentao, Q. Wenwen, Z. Jinxing (2018), "Decreased post-seismic landslides linked to vegetation recovery after the 2008 Wenchuan earthquake", Elsevier Journal on Ecological Indicators, Vol 89, pp 438-444.

[2] A. Roberta, N. Fabrizio, S. Tanya, B. Christian, S. Salvatore, C. Marco, P. Nazarreno. (2018), " Earthquake damage mapping: An overall assessment of good surveys and VHR image change detection after L'Aquila 2009 earthquake", Elsevier Journal on Remote Sensing of Environment, Vol. 210, pp. 166-178.

[3] S. Tazio, K. Jan, F. Holger, C. Rafael, H. Christian, W. Urs, C. R. Alejo (2018), "Satellite SAR interferometry for the improved assessment of the state of activity of landslides: A case study from the Cordilleras of Peru", Elsevier Journal on Remote Sensing of Environment, Vol. 217, pp. 111-125.

[4] D. B. William, L. Y. William, E. M. Daniel (2018), "Induced Earthquake and Liquefaction hazards in Oklahoma, USA: Constraints from InSAR", Elsevier Journal on Remote Sensing of Environment, Vol. 218, pp. 1-12.

[5] S. Giancarlo, V. Cristian, C. Chantel, B. Simone, G. Paolo (2018), "CubeSat constellations for Disaster Management in Remote Areas", Acta Astronautica, Vol. 145, pp 11-17.

[6] G. Christian, J. Marianne, L. Tobia, T. Hannes (2016), "Estimation of Seismic Vulnerability Levels of Urban Structures with Multi sensor Remote Sensing", IEEE Journal of Selected Topics In Applied Earth Observations And Remote Sensing, Vol. 9., No. 5.

[7] G. Y. Kanchikayan, B. T. Zhumbayev, A. V. Streltsov (2016), "Modification of the Ionosphere by Precursors of Strong Earthquakes", The Radio Science Bulletin, Vol. 357.

[8] S. Klonus, D. Tomowski, M. Ehlers, P. Reinartz, U. Michel (2012), "Combined Edge Segment Texture Analysis for the Detection of Damaged Buildings in Crisis Areas", IEEE Journal of Selected Topics in Applied Earth Observations and Remote Sensing, Vol. 5, No. 4.

[9] G. Andre, L. Chiroiu, C. Mering, F. Chopin (2003), "Building destruction and damage assessment after earthquake using high resolution optical sensors. The case of the Gujarat earthquake of January 26, 2001", IEEE.

[10] M. Hosokawa, B. Jeong, O. Takizawa (2009), "Earthquake Intensity Estimation and Damage Detection using Remote Sensing Data for Global Rescue Operations", 978-1-4244-3395-7/09/$25.00 ©2009 IEEE.

[11] S. Stramondo (2013), "The Tohoku–Oki Earthquake: A Summary of Scientific Outcomes from Remote Sensing", IEEE Geoscience and Remote Sensing Letters, Vol. 10, No. 4.

[12] S. J. H. Kazmi (2006), "On the Use of Remote Sensing and GIS Techniques in Post Earthquake Damage Identification and Assessment in Pakistan", presented at an Interdisciplinary International Workshop on Earthquake Risk Management, held in Zurich, Switzerland.

[13] X. Tong, Z. Hong, S. Liu, X. Zhang, H. Xie, Z. Li, S. Yang, W. Wang, F. Bao (2012), "Building-damage detection using pre- and post-seismic high-resolution satellite stereo imagery: A case study of the May 2008 Wenchuan earthquake", ISPRS Journal of Photogrammetry and Remote Sensing.

[14] W. Liu, F. Yamazaki (2013), "Detection of Crustal Movement From TerraSAR-X Intensity Images for the 2011 Tohoku, Japan Earthquake", IEEE Geoscience and Remote Sensing Letters, Vol. 10, No. 1.

[15] X. Tong, X. Lin, T. Feng, H. Xie, S. Liu, Z. Hong, P. Chen (2013), "Use of shadows for detection of earthquake-induced collapsed buildings in high-resolution satellite imagery", ISPRS Journal of Photogrammetry and Remote Sensing.

[16] T. Kobayashi, Y. Morishita, H. Munekane (2018), "First detection of precursory ground inflation of a small phreatic eruption by InSAR", Elsevier Journal of Earth and Planetary Science Letters, Vol 491, pp 244-254.

[17] Roberta Bonni, Massimiliano Bordoni, Alessio Colombo, Luca Lanteri, Claudia Meisina (2018), "Landslide state of Activity Maps by combining multi temporal A-DInSAR data (LAMBDA)", Elsevier Journal of Remote Sensing of Environment, Vol. 217, pp 172-190.

[18] Noelie Bontemps, Pascal Lacroix, Marrie-Pierre Doin (2018), "Inversion of deformation fields time series from optical images and application to the long term kinematics of slow-moving landslides in Peru", Journal of Remote Sensing of Environment, Vol. 210, pp. 144-158.

[19] Pascal Lacroix, Gregory Breviere, Erwan Pathier, Ulrick Kniess, Denis Jongmans (2018), "Use of Sentinel-2 images for the detection of precursory motions before landslide failures", Journal of Remote Sensing of Environment, Vol. 215, pp. 507-516.

[20] Zheng Wang, Zhenog Li, Jon Mills, (2018) "A new approach to selecting coherent pixels for ground-based SAR deformation monitoring", ISPRS Journal of Photogrammetry and Remote Sensing, Vol. 144, pp. 412-422.

[21] Xi Chen, Jing Li, Yunfei Zhang, Weiguo Jiang, Liangliang Tao, Wei Shen (2017), "Evidential Fusion Based Technique for Detecting Landslide Barrier Lakes From Cloud-Covered Remote Sensing Images", IEEE Journal of Selected Topics in Applied Earth Observations and Remote Sensing, Vol. 10, No. 5.

[22] Ning Cao , Hyongki Lee , Evan Zaugg, Ramesh Shrestha, William Carter, Craig Glennie , Guoquan Wang, Zhong Lu, Juan Carlos Fernandez-Diaz (2017), "Airborne DInSAR Results Using Time-Domain Backprojection Algorithm: A Case Study Over the Slumgullion Landslide in Colorado With Validation Using Spaceborne SAR, Airborne LiDAR, and Ground-Based Observations", IEEE Journal of Selected Topics in Applied Earth Observations and Remote Sensing, Vol. 10, No. 11.

[23] Pakhrur Razi, Josaphat Tetuko Sri Sumantyo, Daniele Perissin, Hiroaki Kuze, Ming Yam Chua, Good Fried Panggabean (2018), " 3D Land Mapping and Land Deformation Monitoring Using Persistent Scatterer Interferometry (PSI) ALOS PALSAR: Validated by Geodetic GPS and UAV", IEEE Access, Vol. 6, pp. 12395-12404.

[24] D. Tarchi, D. Leva, N. Casagli, R. Fanti, G. Luzi, M. Pieraccini, A. Pasuto, and S. Silvano (2003), "Landslide monitoring by using ground-based SAR interferometry. An example of application to the Tessina landslide in Italy," Engineering Geology, vol. 68, no. 1/2, pp. 15–30.

[25] M. Crosetto, G. Luzi, O. Monserrat, M. Cuevas (2011), "Ground-based synthetic aperture radar deformation monitoring: Introduction", GeoMonitoring.

[26] M. Sato, Z. Zhou, T. Hamasaki, W. Boerner (2012), "Development of a Ground-based Synthetic Aperture Radar (GB-SAR) system and its applications in Environment Monitoring and Disaster Prevention", Center for Northeast Asian Studies, Tohoku University.

[27] E. Yigit *et. al*. (2012), "Millimeter-wave Ground-based Synthetic Aperture Radar Imaging for Foreign Object Debris Detection: Experimental Studies at Short Ranges", Springer Science + Business Media New York.

[28] A. Ovando, J.M. Martinez, J. Tomasella, D.A. Rodriguez, C. von Randow (2018), "Multi-temporal flood mapping and satellite altimetry used to evaluate the flood dynamics of the Bolivian Amazon wetlands", International Journal of Applied Earth Observation Geoinformation, Vol. 69, pp- 27-40.

[29] Kai Schreoter, Stefan Lüdtke, Richard Redweik, Jessica Meier, Mathias Bochow, Lutz Ross, Claus Nagel, Heidi Kreibich (2018), "Flood loss estimation using 3D city models and remote sensing data", Journal of Environmental Modelling & Software, Vol. 105, pp-118-131.

[30] Lorenzo Alfieri, Sagy Cohen, John Galantowicz, Guy J-P. Schumann, Mark A. Trigg, Ervin Zsoter, Christel Prudhomme, Andrew Kruczkiewicz, Erin Coughlan de Perez, Zachary Flamig, Roberto Rudari, Huan Wu, Robert F. Adler, Robert G. Brakenridge, Albert Kettner, Albrecht Weerts, Patrick Matgen, Saiful A.K.M Islam, Tom de Groeve, Peter Salamon (2018), "A global network for operational flood risk reduction", Journal of Environmental Science and Policy, Vol. 84, pp-149-158.

[31] A.B. Hart, G.J. Hearn (2018), "Mapping geohazards in the watersheds above Leh, Ladakh: The use of publicly-available remote sensing to assist risk management", International Journal of Disaster Risk Reduction, Vol. 31, pp. 789-798.

[32] Moslem Ouled Sghaier, Samuel Foucher, and Richard Lepage (2017), "River Extraction From High-Resolution SAR Images Combining a Structural Feature Set and Mathematical Morphology", IEEE Journal on Selected Topics in Applied Earth Observations and Remote Sensing, Vol. 10, No. 3.

[33] Guoqiang Tang, Ziyue Zeng, Meihong Ma, Ronghua Liu, Yixin Wen, and Yang Hong (2017), "Can Near-Real-Time Satellite Precipitation Products Capture Rainstorms and Guide Flood Warning for the 2016 Summer in South China?", IEEE Geoscience and Remote Sensing letters, Vol. 14, No. 8.

[34] François Mercier, Nawal Akrour, Laurent Barthès, Cécile Mallet, Ruben Hallali (2017), "Fine-Scale Evaluation of Rainfall from TV-Sats: A New Method for Water Monitoring and Flash Flood Prevention", The Radio Science Bulletin.

[35] Keiller Nogueira , Samuel G. Fadel , Ícaro C. Dourado, Rafael de O. Werneck , Javier A. V. Muñoz, Otávio A. B. Penatti , Rodrigo T. Calumby , Lin Tzy Li , Jefersson A. dos Santos , and Ricardo da S. Torres (2018), "Exploiting ConvNet Diversity for Flooding Identification", IEEE Geoscience and Remote Sensing Letters, Vol. 15, No. 9.

[36] D. C. Mason, I. J. Davenport, J. C. Neal, G. J.-P. Schumann, and P. D. Bates (2012), "Near Real-Time Flood Detection in Urban and Rural Areas Using High-Resolution Synthetic Aperture Radar Images", IEEE Transactions on Geoscience and Remote Sensing, Vol. 50, No. 8.

[37] R. Cossu, P. Bally, O. Colin, G. Trianni (2008), "Rapid mapping of flood events through the use of FAIRE (Fast Access to Imagery for Rapid Exploitation)", Geophysical Research Abstracts, Vol. 10.

[38] Muhammad Al-Amin Hoque, Stuart Phinn, Chris Roelfsema, Iraphne Childs (2018), "Assessing tropical cyclone risks using geospatial techniques", Journal of Applied Geography, Vol. 98. pp- 22-33.

[39] Xingru Feng, Mingjie Li, Baoshu Yin, Dezhou Yang, Hongwei Yang (2018), "Study of storm surge trends in typhoon-prone coastal areas based on observations and surge-wave coupled simulations",

International Journal of Applied Earth Observation Geoinformation, Vol. 68, pp- 272-278.

[40] Yanling Du , Wei Song , Qi He , Dongmei Huang , Antonio Liotta , Chen Su (2018)," Deep Learning with Multi-scale Feature Fusion in Remote Sensing for Automatic Oceanic Eddy Detection", Journal of Information Fusion, Accepted manuscript.

[41] Bikash R. Paridaa,⋆, Sailesh N. Beherab, Bakimchandra Oinamc, N.R. Pateld, R.N. Sahooe (2018), "Investigating the effects of episodic Super-cyclone 1999 and Phailin 2013 on hydro-meteorological parameters and agriculture: An application of remote sensing", Journal of Remote Sensing Applications: Society and Environment, Vol. 10, pp. 128-137.

[42] Anoop Kumar Mishra (2018), "Remote sensing of convective clouds using multi-spectral observations and examining their variability over India", Journal of Remote Sensing Applications: Society and Environment, Vol. 12, pp. 23-29.

[43] Shaohui Jin, ShuangWang, Xiaofeng Li, Senior Member, IEEE, Licheng Jiao, Senior Member, IEEE, Jun A. Zhang, Senior Member, IEEE, and Dongliang Shen, Student Member, IEEE (2017), "A Salient Region Detection and Pattern Matching-Based Algorithm for Center Detection of a Partially Covered Tropical Cyclone in a SAR Image", IEEE Transactions on Geoscience and Remote Sensing, Vol. 55, No. 1.

[44] Yuan Ma, Xiaolei Zou, Member, IEEE, and Fuzhong Weng (2017), "Potential Applications of Small Satellite Microwave Observations for Monitoring and Predicting Global Fast-Evolving Weathers", IEEE Journal of Selected Topics in Applied Earth Observation and Remote Sensing, Vol. 10, No. 6.

[45] Tangao Hu , Xiao Wang, Dengrong Zhang, Gang Zheng , Yuzhou Zhang, Yiyue Wu, and Bin Xie (2017), "Study on Typhoon Center Monitoring Based on HY-2 and FY-2 Data", IEEE Geoscience and Remote Sensing Letters, Vol. 14, No.12.

[46] A. Wada, N. Usui, K. Sato (2012), "Relationship of maximum tropical cyclone intensity to sea surface temperature and tropical cyclone heat potential in the North Pacific Ocean", Journal of Geophysical Research, Vol. 117.

[47] B. B. Barnes, C. Hu (2013), "A Hybrid Cloud Detection Algorithm to Improve MODIS Sea Surface Temperature Data Quality and Coverage Over the Eastern Gulf of Mexico", IEEE Transactions on Geoscience and Remote Sensing, Vol 51, No. 6.

[48] D. Das A. Maitra (2012), "Time series prediction of rain rate during rain events at a tropical location", Published in IET Microwaves, Antennas & Propagation.

[49] M. M. Ali, D. Swain, T. Kashyap, J. P. McCreary, P. V. Nagamani (2013), "Relationship Between Cyclone Intensities and Sea Surface Temperature in the Tropical Indian Ocean", IEEE Geoscience and Remote Sensing Letters, Vol. 10, No. 4.

[50] N. Jaiswal, C. M. Kishtawal (2013), "Objective Detection of Center of Tropical Cyclone in Remotely Sensed Infrared Images", IEEE Journal of Selected Topics in Applied Earth Observations and Remote Sensing, Vol. 6, No. 2.

[51] R. Romeiser, J. Horstmann, M. J. Caruso, H. C. Graber (2013), "A Descalloping Postprocessor for ScanSAR Images of Ocean Scenes", IEEE Transactions on Geoscience and Remote Sensing, Vol 51, No. 6.

[52] Changzhan Gu, Zhengyu Peng, Changzhi Li (2016), "High-Precision Motion Detection Using Low-Complexity Doppler Radar With Digital Post-Distortion Technique", IEEE Transactions on Microwave Theory and Techniques, Vol. 64, No. 3.

[53] Jianxuan Tu, Taesong Hwang, Jenshan Lin (2016), "Respiration Rate Measurement Under 1-D Body Motion Using Single Continuous-Wave Doppler Radar Vital Sign Detection System", IEEE Transactions on Microwave Theory and Techniques, Vol. 64, No. 6.

[54] Yong Wang, Yuanjin Zheng (2017), "An FMCW Radar Transceiver Chip for Object Positioning and Human Limb Motion Detection", IEEE Sensors Journal, Vol. 17, No. 2.

[55] Chuanwei Ding, Li Zhang, Chen Gu, Lei Bai, Zhicheng Liao, Hong Hong , Yusheng Li, Xiaohua Zhu (2018), "Non-Contact Human Motion Recognition Based on UWB Radar", IEEE Journal on Emerging Trends and Selected Topics in Circuits and Systems, Vol. 8, No. 2.

[56] Robert H. Nakata, Brian Haruna, Takashi Yamaguchi, Victor M. Lubecke, Shigeru Takayama, Kiyotsugu Takaba (2018), "Motion Compensation for an Unmanned Aerial Vehicle Remote Radar Life Sensor", IEEE Journal on Emerging Trends and Selected Topics in Circuits and Systems, Vol. 8, No. 2.

[57] A. Marino, S. R. Cloude, J. M. Lopez-Sanchez (2013), "A New Polarimetric Change Detector in Radar Imagery", IEEE Transactions on Geoscience and Remote Sensing, Vol. 51, No. 5.

[58] M. Vahidpour, K. Sarabandi (2012), "Millimeter-Wave Doppler Spectrum and Polarimetric Response of Walking Bodies", IEEE Transactions on Geoscience and Remote Sensing, Vol. 50, No. 7.

[59] P. Chen, M. C. Shastry, C. Lai, R. M. Narayanan (2012), "A Portable Real-Time Digital Noise Radar System for Through-the-Wall Imaging", IEEE Transactions on Geoscience and Remote Sensing, Vol. 50, No. 10.

[60] P. F. Sammartino, C. J. Baker, and M. Rangaswamy (2008), "Moving target localization with multistatic radar systems," in Proceedings of IEEE Radarcon, May 26–30.

[61] Y. Liu, Y. Deng (2012), "CARMSAR-a Compact and Reconfigurable Miniature SAR system for High Resolution Remote Sensing".

[62] Y. Xu, S. Wu, C. Chen, J. Chen, and G. Fang (2012), "A Novel Method for Automatic Detection of Trapped Victims by Ultra-wideband Radar", IEEE Transactions on Geoscience and Remote Sensing, Vol. 50, No. 8.